

# Journal of Visualized Experiments

## Visualization of Amyloid beta Deposits in Human Brain with Matrix-assisted Laser Desorption/Ionization Imaging Mass Spectrometry --Manuscript Draft--

<b>Article Type:</b>	Invited Methods Article - JoVE Produced Video
<b>Manuscript Number:</b>	JoVE57645R4
<b>Full Title:</b>	Visualization of Amyloid beta Deposits in Human Brain with Matrix-assisted Laser Desorption/Ionization Imaging Mass Spectrometry
<b>Keywords:</b>	MALDI-imaging mass spectrometry, human autopsy brain, Amyloid $\beta$ , Alzheimer's disease, senile plaques, cerebral amyloid angiopathy
<b>Corresponding Author:</b>	Masaya Ikegawa Doshisha Daigaku Seimei Ikagakubu Daigakuin Seimei Ikagaku Kenkyuka Kyotanabe, JAPAN
<b>Corresponding Author's Institution:</b>	Doshisha Daigaku Seimei Ikagakubu Daigakuin Seimei Ikagaku Kenkyuka
<b>Corresponding Author E-Mail:</b>	mikegawa@mail.doshisha.ac.jp
<b>Order of Authors:</b>	Masaya Ikegawa Takashi Nirasawa Nobuto Kakuda Tomohiro Miyasaka Shigeo Murayama Yasuo Ihara Yuki Kuzuhara
<b>Additional Information:</b>	
<b>Question</b>	<b>Response</b>
Please indicate whether this article will be Standard Access or Open Access.	Open Access (US\$4,200)
Please indicate the <b>city, state/province, and country</b> where this article will be <b>filmed</b> . Please do not use abbreviations.	1-3 Tatara-Miyakodani, Kyotanabe City, Kyoto, Japan

**TITLE:**

**Visualization of Amyloid  $\beta$  Deposits in the Human Brain with Matrix-assisted Laser Desorption/Ionization Imaging Mass Spectrometry**

**AUTHORS AND AFFILIATIONS:**

Masaya Ikegawa<sup>1</sup>\*, Takashi Nirasawa<sup>2</sup>\*, Nobuto Kakuda<sup>1</sup>, Tomohiro Miyasaka<sup>1</sup>, Yuki Kuzuhara<sup>1</sup>, Shigeo Murayama<sup>3</sup>, Yasuo Ihara<sup>4</sup>

<sup>1</sup>Department of Life and Medical Systems, Doshisha University, Kyoto, Japan

<sup>2</sup>Bruker Daltonics K.K., Yokohama, Japan

<sup>3</sup>The Brain Bank for Aging Research, Tokyo Metropolitan Geriatric Hospital and Institute of Gerontology, Tokyo, Japan

<sup>4</sup>Graduate School of Brain Science, Doshisha University, Kyoto, Japan

\* These authors contributed equally to this work.

**Corresponding Author:**

Masaya Ikegawa (mikegawa@mail.doshisha.ac.jp)

**E-mail Addresses of the Co-authors:**

Takashi Nirasawa (takashi.nirasawa@bruker.com)

Nobuto Kakuda (nkakuda@mail.doshisha.ac.jp)

Tomohiro Miyasaka (tomiyasa@mail.doshisha.ac.jp)

Yuki Kuzuhara (yu.xix92@gmail.com)

Shigeo Murayama (smurayam@gmail.com)

Yasuo Ihara (yihara0216@gmail.com)

**KEYWORDS:**

MALDI-imaging mass spectrometry, human autopsy brain, amyloid  $\beta$ , Alzheimer's disease, senile plaques, cerebral amyloid angiopathy

**SUMMARY:**

Molecular imaging with matrix-assisted laser desorption/ionization-based imaging mass spectrometry (MALDI-IMS) allows the simultaneous mapping of multiple analytes in biological samples. Here, we present a protocol for the detection and visualization of amyloid  $\beta$  protein on brain tissues of Alzheimer's disease and cerebral amyloid angiopathy samples using MALDI-IMS.

**ABSTRACT:**

The neuropathology of Alzheimer's disease (AD) is characterized by the accumulation and aggregation of amyloid  $\beta$  (A $\beta$ ) peptides into extracellular plaques of the brain. The A $\beta$  peptides, composed of 40 amino acids, are generated from amyloid precursor proteins (APP) by  $\beta$ - and  $\gamma$ -secretases. A $\beta$  is deposited not only in cerebral parenchyma but also in leptomeningeal and cerebral vessel walls, known as cerebral amyloid angiopathy (CAA). While a variety of A $\beta$  peptides were identified, the detailed production and distribution of individual A $\beta$  peptides in pathological

tissues of AD and CAA have not been fully addressed. Here, we develop a protocol of matrix-assisted laser desorption/ionization-based imaging mass spectrometry (MALDI-IMS) on human autopsy brain tissues to obtain comprehensive protein mapping. For this purpose, human cortical specimens were obtained from the Brain Bank at the Tokyo Metropolitan Institute of Gerontology. Frozen cryosections are cut and transferred to indium-tin-oxide (ITO)-coated glass slides. Spectra are acquired using the MALDI system with a spatial resolution up to 20  $\mu\text{m}$ . Sinapinic acid (SA) is uniformly deposited on the slide using either an automatic or a manual sprayer. With the current technical advantages of MALDI-IMS, a typical data set of various A $\beta$  species within the same sections of human autopsied brains can be obtained without specific probes. Furthermore, high-resolution (20  $\mu\text{m}$ ) imaging of an AD brain and severe CAA sample clearly shows that A $\beta$ 1-36 to A $\beta$ 1-41 were deposited into leptomeningeal vessels, while A $\beta$ 1-42 and A $\beta$ 1-43 were deposited in cerebral parenchyma as senile plaque (SP). It is feasible to adopt MALDI-IMS as a standard approach in combination with clinical, genetic, and pathological observations in understanding the pathology of AD, CAA, and other neurological diseases based on the current strategy.

## INTRODUCTION:

In order to make the diagnosis and to understand the pathogenesis of neurodegenerative disorders, precise molecular identification of pathological deposits is essential<sup>1</sup>. In the course of AD, A $\beta$  is produced to make SPs in the cerebral parenchyma and deposited in vessels long before disease onset<sup>2-6</sup>. While A $\beta$ 1-42 is the predominant peptide in the SP of AD brains, other A $\beta$  variants, such as N-terminal or C-terminal truncated or modified A $\beta$ s, are also identified in affected AD brains<sup>7-10</sup>. A full picture of the broad range of A $\beta$  species in human brains, especially with AD and cerebral amyloid angiopathy (CAA)<sup>11</sup>, will help scientists understand A $\beta$  production, metabolism, and deposition.

As the classical approach of neuropathology, immunohistochemistry (IHC) has been the most conclusive method to determine the location of A $\beta$ s in the brain tissues<sup>12-15</sup>. In general, IHC cannot distinguish molecules when several epitopes coexist simultaneously. By contrast, an emerging mass spectrometry-based proteomic analysis is a valuable approach especially for analyzing a variety of A $\beta$  species in brain tissues, which cannot be differentiated with antibodies<sup>16,17</sup>. The conventional mass spectrometry-based analysis of brain lysates and immunoprecipitated samples fails to detect minor A $\beta$  peptides and loses distribution information of A $\beta$  in the brain tissue.

In earlier works, visualizing A $\beta$  deposits in mouse brains has been successful using a transgenic animal model of AD, such as APP23. However, this process still needs technical advancements to compare IMS and IHC with respect to resolution and sensitivity<sup>18-20</sup>. AD neuropathology should be studied on human brains, and we used MALDI-IMS technology on human autopsy brain tissues to obtain comprehensive protein mapping<sup>21</sup>. For this purpose, we developed a protocol for an advanced type of mass spectrometry that has advantages in its rapidity, sensitivity, and reproducibility.

## PROTOCOL:

Here, tissue samples were collected at the Tokyo Metropolitan Geriatric Hospital, which provides community-based medical services to the elderly population in Japan. The brain autopsy samples used in the study were registered to the Brain Bank for Aging Research (BBAR) with the informed consent of the deceased's relatives. The BBAR is approved by the ethics committee of the Tokyo Metropolitan Geriatric Hospital and Institute of Gerontology. For all brains registered at the brain bank, we obtained written informed consents for their use for medical research from the patients or their families. The patients were placed in a cold (4 °C) room within 2 h after death to reduce postmortem changes in the brain. All methods described here have been approved by Doshisha University and the Brain Bank for Aging Research, Tokyo Metropolitan Geriatric Hospital and Institute of Gerontology.

## **1. Preparation of Tissue Sections for IMS**

### **1.1. Processing tissue specimen of a human autopsied brain**

Note: Ensure that the sample preparation step for IMS preserves the original state of the tissue. Avoid contamination and post-mortem changes. The following step is crucial.

1.1.1. Obtain human cortical specimens for IMS from brains that were removed, processed, and stored at -80 °C within 8 h postmortem. Take the brain specimen from the occipital cortex of AD patients and age-matched controls<sup>21</sup>.

### **1.2. Preparation of frozen tissue sections**

1.2.1. Cut the tissue sections on a cryostat. Place conductive ITO-coated microscope glass slides inside the cryostat<sup>21</sup>.

1.2.2. Warm the autopsy brain specimen from -80 °C to -22 °C inside the cryostat.

1.2.3. Attach a new disposable blade to the cryostat for every experiment. Always try to use a clean part of the blade.

1.2.4. Put the frozen autopsy brains on the stage along with a small amount of OCT compound (enough to cover the central area of the stage; see **Table of Materials**).

1.2.5. Choose the conditions for thin sectioning. For IMS, use a thickness of 10 - 12 µm for human brain sections. For IMS and IHC, cut five to six sections from each tissue sample.

1.2.6. When the blade is just starting to cut the tissue, turn the wheel and "face" the block until all of the tissue is exposed. If there is a small streak or tear across the section, wait a little more in the cryostat until the temperature adjustment automatically fixes it. Count a few seconds before opening the anti-roll with a tissue underneath.

1.2.7. Immediately place the tissue slice on the ITO-coated side of the glass slide. Thaw the tissue slice by putting a finger underneath the slide on the non-ITO-coated side. The tissue will stick to the slide; ensure that the tissue is as flat as possible with no wrinkles. Perform this step at room temperature.

Note: Wear gloves, masks, and a laboratory gown because the human samples may contain biological contaminants. When all sections have been made for the day, clean the cryostat, brushes, and chucks with laboratory wipes and 200 mL of 100% ethanol.

### 1.3. Rinsing the tissue sections

1.3.1. Immerse the samples in 40 - 100 mL of 70% ethanol for 30 s to remove endogenous lipids and inorganic salts. Use a glass staining jar.

1.3.2. Wash the samples with 40 - 100 mL of 100% ethanol for 30 s, 40 - 100 mL of Carnoy's solution for 3 min, 40 - 100 mL of 100% ethanol for 30 s, 40 - 100 mL of 0.1% trifluoroacetic acid (TFA) for 1 min, and 40 - 100 mL of 100% ethanol for 30 s. Use a glass staining jar.

Note: Carnoy's solution is a fixative composed of six parts ethanol, three parts acetic acid, and one part chloroform.

1.3.3. Dry in a vacuum for 30 min.

### 1.4. Treatment of the tissue sections with a formic acid vapor for a better ionization of the A $\beta$ proteins from autopsy brain tissues

1.4.1. Prepare the oven and incubation glass slide to be used for the subsequent vaporization with 5 mL of 100% formic acid. To achieve a satisfactory acid treatment, keep the air humidity in the incubation glass dish at saturation level throughout this step and keep the temperature at 60 °C. Place the tissue slides in the incubation glass dish while avoiding submersion in the formic acid and treat for 6 min.

1.4.2. Take an optical image of the samples using a film scanner, gel scanner, or a digital microscope, etc. Perform this step at room temperature. The alignment of the optical image of the samples is necessary when the sample target is placed inside the instrument. Usually, it will not be possible to recognize the tissue section underneath the matrix layer.

Note: The most convenient way to take an optical image is to use an office scanner. It is a good idea to save the image in the imaging data storage folder.

1.4.3. To correlate the optical images with the samples, make guide marks that are visible both in the optical image and underneath the matrix layer in the camera optic. The easiest way is to spot at least three correction fluid marks around the sample before taking the optical image.

## 1.5. Matrix application

### 1.5.1. Preparation of the matrix solution

1.5.1.1. In an organic solvent-tolerant microtube, prepare a 10 mg/mL SA solution in 50% acetonitrile (ACN) and 0.1% TFA. Thoroughly dissolve the SA compound by vortexing or brief sonication for 10 min. Store the solution at room temperature until use.

Note: There are three different options for matrix spraying: using an airbrush, an ultrasonic sprayer, or an automatic sprayer.

### 1.5.2. Spraying the matrix with an airbrush

1.5.2.1. Perform the operation at a constant room temperature (20 - 23 °C) and humidity (40% - 60%). The parameters to adjust for optimal spraying include the size of the droplet, the amount of mist, the angle and distance between the spray nozzle and the tissue section, and the laboratory temperature and humidity. Adjust these conditions by checking the microscopy results.

Note: As limiting factors include the crystal size and homogeneity of the matrix coverage and the undesirable migration/diffusion of analytes, smaller is better for the drop size. Homogeneity is also the point of inspection.

### 1.5.3. Spraying the matrix with an ultrasonic sprayer

1.5.3.1. Remove the tissue to be sprayed from the desiccator and place it in the chamber. Make sure the tissue is not covering the sensor window.

1.5.3.2. Start the preparation by pushing the **Start** button; usually, prep time is around 90 min. The preparation will be regulated automatically *via* the monitoring of the matrix layer thickness and wetness. After the preparation is complete, remove the slide and store it in the desiccator for 15 min before reading it in the MALDI instrument.

1.5.3.3. Clean the sprayer with 2 - 3 mL of 100% MeOH until the spray head appears clean.

Note: A fine mist of matrix droplets is allowed to sink into the tissue by a gravitational sheet. An average droplet size of 20 µm is generated; all droplet diameters are less than 50 µm.

### 1.5.4. Spraying the matrix with an automatic sprayer

1.5.4.1. Spray the matrix solution on the tissue surface with an automatic sprayer. A constant flow of heated sheath gas (N<sub>2</sub>, set at 10 psi and 75 °C) will be delivered conjointly with the matrix solution spray. Use a solvent pump system (set at 10 psi and 0.15 mL/min) to deliver the matrix solution.

Note: Most importantly, work under a safety cabinet to avoid any inhalation of matrix aerosols. Control the room temperature and humidity to reproduce homogenous matrix crystallization.

## 2. MALDI-IMS

### 2.1. Perform ultra-high-speed mass spectrometry.

2.1.1. Perform high-throughput and high-spatial-resolution imaging experiments with MALDI-IMS equipped with a 10 kHz Nd:YAG (355 nm) laser.

2.1.2. For mass spectrometry measurements, define the tissue areas using the MALDI control software and data analysis software.

2.1.3. Acquire spectra in a positive linear mode with a mass range of  $m/z$  2,000 - 20,000 and a spatial resolution of 20 and 100  $\mu\text{m}$ .

2.1.4. To make the calibration standard, dissolve the peptide calibration standard and the protein calibration standard with a ratio of 1:4 with alpha-Cyano-4-hydroxyl-cinnamic acid (CHCA) in TA30 solution (ACN:0.1% TFA = 30:70) and then dilute it 10x. Place 1  $\mu\text{L}$  of calibration standard on the slide at four different locations.

2.2. Using molecular histology software (see **Table of Materials**), overlay multiple single images to find the spatial correlation of various signals, such as different A $\beta$  peptides colocalizing in SPs and arterial walls.

## 3. Data Processing

3.1. For spectral alignment, align all spectra to a selected  $m/z$  list from a previous publication<sup>21</sup>.

3.2. Import the MALDI-IMS data set into statistical analysis software (see **Table of Materials**) with baseline subtraction.

3.3. Trace regions of interest (ROIs) based on histological knowledge.

3.3.1. Perform a univariate analysis for the mean intensities, standard deviations, uncovering of discriminative  $m/z$ -markers (ROC analysis), hypothesis tests, and discovery of colocalized  $m/z$  values.

3.4. Create a segmentation map.

3.4.1. Perform an unsupervised multivariate analysis for the spatial segmentation of large datasets and a component analysis for the extraction of underlying trends.

3.4.2. Select anatomical ROIs based on histological characteristics, such as parenchyma and the subarachnoid space.

3.4.3. Assign structures as individual ROIs and correlate them with the processed MS data in order to identify the associated peptides that allowed the image segmentation of the region.

#### REPRESENTATIVE RESULTS:

Sporadic AD patients with CAA ( $n = 5$ ; mean age = 83.2 y) and aged subjects with senile plaque free (SP O) and CAA ( $n = 5$ ; mean age = 77.2 y) were analyzed (**Table 1**). The CAA phenotypes of patient #3 were most prominent in this study. Distributions of A $\beta$ 1-40 and A $\beta$ 1-42 deposits in the brain tissue from patient #3 were visualized with MALDI-IMS (**Figure 1**). There were no significant signals in nonpathological control brains (patients #9 and #10), as shown in **Figure 1**. Here, MALDI-IMS clearly visualized that A $\beta$ 1-42 was preferentially deposited as SPs in the cerebral parenchyma. By contrast, shorter A $\beta$ s, such as A $\beta$ 1-36 to 1-41, were preferentially deposited on the leptomeningeal vascular areas (**Figure 1**).

Distributions of A $\beta$ 40 and A $\beta$ 42 were further validated with IHC using adjacent frozen sections of the tissues. The anti-A $\beta$ 40 antibody labeled CAA (arrows in **Figure 2B**), which is in clear contrast to the distribution of A $\beta$ 42 in the cerebral parenchyma as SPs. For A $\beta$ 1-41, we are the first to detect this fragment in human brains, and we have generated specific antibodies that can differentiate A $\beta$ 41 from A $\beta$ 40 and A $\beta$ 42<sup>21</sup>.

The spatial resolution of the MALDI-IMS is generally the most important factor to be improved upon. In **Figure 1** and **Figure 2** show MALDI-IMS with a 100  $\mu$ m pitch resolution and obtain an overall distribution profile for a relatively wide area<sup>21</sup>. It is difficult to define amyloid deposition exactly at the subarachnoid space, including vascular structure. To portray fine tissue structures of subarachnoid vessels and the surface of the cortex, high-resolution MALDI imaging (40  $\mu$ m: **Figure 3**; 20  $\mu$ m: **Figure 4** and **Figure 5**) was performed. As a result, MALDI-IMS clearly demonstrated that shorter A $\beta$ s, such as A $\beta$ 1-36 to 1-41, are distributed in the walls of arteries, which is comparable with IHC.

MALDI-IMS demonstrated the detailed distributions of both A $\beta$ <sub>x</sub>-40 and A $\beta$ <sub>x</sub>-42 ( $x = 2, 4, 5, 6, 7, 8, 9$ , and 11pE) in AD accompanied with moderate CAA brain. For example, while A $\beta$ <sub>x</sub>-40 species showed a similar distribution profile to A $\beta$ 1-40, A $\beta$ <sub>x</sub>-42 species showed a different distribution pattern with A $\beta$ 1-42<sup>21</sup>. By the current protocol, single ion images of the individual A $\beta$  peptides observed with MALDI-IMS are assigned to A $\beta$  species. By contrast, acquired image data can be investigated using unsupervised multivariate statistics in order to obtain image segmentation of anatomical regions of interest for the further analysis of undefined proteins. **Figure 5** shows a segmentation map obtained with a bisecting k-means analysis applied to the same section from patient #3<sup>21</sup>. This clustering method successfully identified plaque-like structures in the parenchyma (blue in **Figure 5C**) and vascular structures in the subarachnoid space (green in **Figure 5C**). It is interesting to find a small circular area in the parenchyma, which is detected just around a small arteriole in the parenchyma, as well as in the subarachnoid space (purple in **Figure 5C**). This is verified by single ion images of these individual A $\beta$  peptides in **Figure 5D - 5F**.



## FIGURE AND TABLE LEGENDS:

**Figure 1: MALDI-IMS of a frozen AD/CAA brain section.** Various C-terminal truncated A $\beta$  peptides in AD accompanying severe CAA (patient #3) are visualized in the left panel and controls (patient #9 on the right and patient #10 on the left in all images) in the right panel. A $\beta$ 1-36 to A $\beta$ 1-41 are preferentially deposited in leptomeningeal blood vessels, while A $\beta$ 1-42 and A $\beta$ 1-43 are deposited in the cerebral parenchyma as senile plaques in case #3, while there was no signal in the control patients' brains (cases #9 and #10). The resolution = 100  $\mu$ m. The scale bar = 5 mm. This figure has been modified with permission from Kakuda *et al.*<sup>21</sup>.

**Figure 2: MALDI-IMS of frozen AD/CAA brain sections and adjacent sections of the occipital cortex from AD brains.** (A - C) The frozen AD/CAA brain sections and (D and E) adjacent sections of the occipital cortex from AD brains were immune-stained and focused on arteriole and cerebral parenchyma, using antibodies against A $\beta$ 40 (D: BA27) or A $\beta$ 42 (E: anti-A $\beta$ 42 polyclonal). Both analyses demonstrated that A $\beta$ 40 is preferentially deposited in leptomeningeal blood vessels (arrows in panel D) and arterioles in the subarachnoid space and the cerebral parenchyma forming CAA. In contrast, A $\beta$ 42 is mainly deposited in SPs. For IMS, the resolution = 100  $\mu$ m. The scale bar for panels A, B, and C (shown in panel A) = 5 mm, and the scale bar for panels D and E (shown in panel D) = 500  $\mu$ m. This figure has been modified with permission from Kakuda *et al.*<sup>21</sup>.

**Figure 3: MALDI-IMS of frozen AD/CAA brain sections (patient #3) at a resolution of 40  $\mu$ m.** Various C-terminal and N-terminal truncated and modified A $\beta$  peptides in AD accompanying severe CAA (patient #3). A $\beta$ 1-36 to A $\beta$ 1-41 are preferentially deposited in leptomeningeal blood vessels, while A $\beta$ 1-42 and A $\beta$ 1-43 are deposited in the cerebral parenchyma as senile plaques. The scale bars = 1 mm, except the upper left, where the scale bar = 2 mm. The resolution = 40  $\mu$ m.

**Figure 4: MALDI-IMS of frozen AD/CAA brain sections (patient #3) at a resolution of 20  $\mu$ m.** This panel shows various C-terminal and N-terminal truncated and modified A $\beta$  peptides in AD accompanying severe CAA (patient #3). A $\beta$ 1-36 to A $\beta$ 1-41 are preferentially deposited in leptomeningeal blood vessels, while A $\beta$ 1-42 and A $\beta$ 1-43 are deposited in the cerebral parenchyma as senile plaques. The scale bars = 200  $\mu$ m, except the upper left, where the scale bar = 1 mm. The resolution = 20  $\mu$ m.

**Figure 5: Segmentation map, obtained by MALDI-IMS of a frozen AD brain section, reveals putative senile plaque, large subarachnoid vessel structures, and small parenchymal arterioles.** (A) Segmentation map obtained from a multivariate image analysis of MALDI-IMS data. (B) Bisecting k-means based clustering analysis identified plaque-like and vessel-like structures in the occipital cortex. The clusters and substructures and their relations are shown as nodes (*e.g.*, 1-0-0). (C) Distinct A $\beta$  peptide localization patterns resembling plaques (blue), subarachnoid vessels (green), and arteriole (red) structures. Note that a few red clusters are also distributed in the subarachnoid space. This is verified by single ion images of these individual A $\beta$  peptides at a 20  $\mu$ m resolution: (D) A $\beta$  1-40, (E) A $\beta$  1-41, and (F) A $\beta$  1-42.

**Table 1: Clinical and pathological data of AD with CAA cases and aged SP O subjects.** Human cortical specimens for IMS and IHC were obtained from the Brain Bank at Tokyo Metropolitan Institute of Gerontology. Each brain specimen was taken from the occipital cortex of five AD patients and five age-matched controls. The extent of amyloid deposition as shown by an A $\beta$  monoclonal antibody was defined by Braak SP (amyloid) stages. At stage O, there are almost no senile plaques throughout the isocortex. At stage C, virtually all the isocortical areas are affected. AD brains are invariable at stage C. This table has been modified with permission from Kakuda *et al.*<sup>21</sup>.

## DISCUSSION:

Here we demonstrated a detailed protocol and results of the visualization of A $\beta$  and its isoforms from several autopsied brains with AD and CAA with MALDI-IMS. The deposition profile of A $\beta$ s was drastically changed from A $\beta$ 1-42 to its N- and C-terminal variations. A $\beta$ 1-41 was first identified and visualized in human brains with the current protocol and was further validated with IHC<sup>21</sup>. Considering that the morphology of deposited A $\beta$  by IMS with a high-resolution analysis (20  $\mu$ m) must be in good agreement with IHC, IMS and IHC equally contribute to distinguishing A $\beta$  deposits by their location and protein contents, as well as by their morphology. As the entire experiment described here was conducted in the occipital cortex, studying the localization of different beta-amyloid species across all brain regions will be generalized with future experiments using the current protocol.

Critical steps within the protocol are tissue preparation steps to obtain an effective ionization of aggregated proteins in human brain tissues. A matrix layer is required to absorb the laser energy and induce desorption and ionization of analytes. In this process, an entire tissue section is homogeneously coated with small crystals. Homogenous cocrystallization of the analyte with the matrix is crucial for high-sensitivity and artifact-free imaging. Each of the three spray methods has its own advantages. Manual spray coating is one of the most frequently used methods. An airbrush is convenient; however, it requires skillful operation. As precise and reproducible experimental technique is essential, using an ultrasonic sprayer and/or an automatic sprayer as described in the current protocols is recommended. With respect to an ultrasonic sprayer, it will not be influenced by the humidity and temperature of the room because it is sprayed into a chamber. Meanwhile, with an automatic sprayer, relatively preserved spatial resolution with good reproducibility is obtained. Generally, the spatial resolution obtained with the three methods increase in the order of 1) airbrush, 2) automatic device, and 3) ultrasonic sprayer.

Most importantly, this protocol was originally generated to detect and visualize A $\beta$ s in human autopsied brain samples. The visualization of A $\beta$ s with MALDI-IMS for APP23 mice, which is generated as an animal model of AD based on the Swedish-type mutation of human APP, has been reported earlier by others with an existing method<sup>18,19</sup>. However, the former protocol applied to APP23 was not sufficient to visualize A $\beta$  in its lateral resolution and sensitivity. Earlier works discussed that high A $\beta$  concentrations outside the tissue boundary are clearly artifacts in APP23 imaging with their protocol<sup>18,19</sup>. That means the so-called 'blur' between real SPs and IMS images due to the matrix extraction step was inevitable with MALDI-type imaging. However, in

the current protocol, the blur disappeared and each spectrum represented every single SP in the brain parenchyma.

As shown here, we can trace A $\beta$ 1-41 for the first time in AD and CAA brains with MALDI-IMS, as well as with IHC, with a specific antibody by our own generation<sup>21</sup>. According to the A $\beta$  processing model, A $\beta$ 1-38 derives from A $\beta$ 1-45 *via* A $\beta$ 1-42, while A $\beta$ 1-41 derives from A $\beta$ 1-45 by  $\gamma$ -secretase stepwise cleavage<sup>27-31</sup>. This means that the current protocol supports this model. As for the limitations of this technique, we must consider the heterogeneity of the samples from human autopsy brain. The most critical step, in a sense, is to assess qualified autopsy brain tissue with ethical proof. With the current protocol on those qualified autopsy brain tissues, MALDI-IMS can individually track the whole distribution of the complex molecules having multiple modifications, as well as unknown factor(s) regulating the pathogenesis of AD, that are yet to be defined. Furthermore, in understanding the overall pathogenesis of various neuropathology in aged human brains, it must be feasible to adopt MALDI-IMS as a standard approach, in combination with clinical, genetic, and pathological observations in neurological diseases.

Another critical step of MALDI-IMS is the data mining process from the obtained data set, which is always time-consuming. Manual data mining of each peak distribution requires the users to click through every image and look for distributions that may correlate to the morphology of the analyzed sample. Automatic spatial segmentation can be used as the first step of data mining, providing an overview of the data set and allowing the quick detection of prominent features. In this approach, similarities between spectra of a given region are statistically determined, and similar spectra are grouped into one cluster. All pixels are color-coded according to their cluster assignment (**Figure 5**). In the present AD/CAA study, the area of interest is the space of A $\beta$  depositions in parenchymal plaque and the subarachnoid and parenchymal vascular structures. The two distinctive peaks which were further validated with IHC were the m/z values from A $\beta$ 1-40 and A $\beta$ 1-42<sup>21</sup>. Thus, it is easy to find colocalized m/z with A $\beta$ 1-40 and A $\beta$ 1-42 which was already annotated to N- and C-terminal truncated A $\beta$ , as well as unknown peptides, for further analysis.

Weller and colleagues have reported that A $\beta$  accumulates in vessel walls, more around arteries than around veins<sup>21</sup>. Moreover, it has been proposed that the interstitial fluid (ISF) includes A $\beta$ s excreted from the cerebral parenchyma to the lymph node *via* a perivascular drainage pathway<sup>22-26</sup>. The current protocol to generate a segmentation map based on a MALDI-IMS data set at a 20  $\mu$ m resolution supports the possible existence of perivascular drainage pathways of the brain (**Figure 5**), which contribute significantly to CAA in AD<sup>21,32</sup>. Furthermore, we can discover marker proteins colocalized with plaque and subarachnoid vasculature by calculating the correlation of each m/z values. In understanding the overall pathogenesis of various neuropathology in aged human brains, it must be feasible to adopt MALDI-IMS as a powerful approach in combination with established IHC data of clinical, genetic, and pathological observations in neurological diseases.

#### ACKNOWLEDGMENTS:

This work was supported in part by the Grant-in-Aid for Scientific Research on Innovative Areas (Brain Protein Aging and Dementia Control 26117004; to M.I. and T.M.). This research was partially supported by the Strategic Research Program for Brain Sciences from the Japan Agency for Medical Research and Development (AMED). All experiments were conducted in compliance with the ARRIVE guidelines.

#### **DISCLOSURES:**

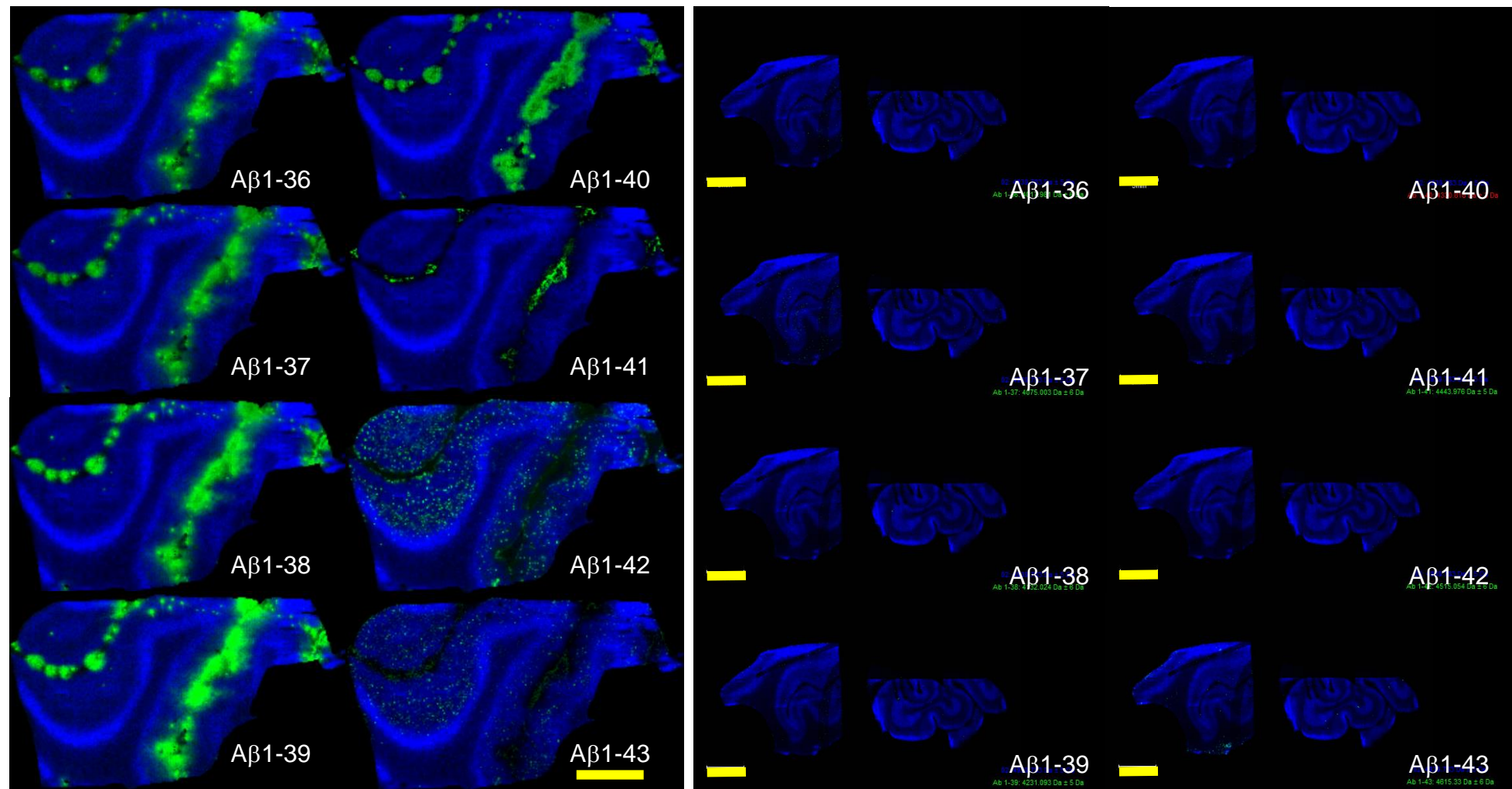
The authors have nothing to disclose.

#### **REFERENCES**

1. Kovacs, G.G. Molecular Pathological Classification of Neurodegenerative Diseases: Turning towards Precision Medicine. *International Journal of Molecular Sciences*. **17**, E189 (2016).
2. Selkoe, D.J. Alzheimer's disease: genes, proteins, and therapy. *Physiological Reviews*. **81**, 741-766 (2001).
3. Selkoe, D.J., Hardy, J. The amyloid hypothesis of Alzheimer's disease at 25 years. *EMBO Molecular Medicine*. **8**, 595-608 (2016).
4. Braak, H., Braak, E. Neuropathological staging of Alzheimer-related changes. *Acta Neuropathologica*. **82**, 239-259 (1991).
5. Braak, H., Alafuzoff, I., Arzberger, T., Kretzschmar, H., Del Tredici, K. Staging of Alzheimer disease-associated neurofibrillary pathology using paraffin sections and immunocytochemistry. *Acta Neuropathologica*. **112**, 389-404 (2006).
6. Bateman, R.J. *et al.* Dominantly Inherited Alzheimer Network. Clinical and biomarker changes in dominantly inherited Alzheimer's disease. *The New England Journal of Medicine*. **367**, 795-804 (2012).
7. Iwatsubo, T. *et al.* Visualization of A beta 42(43) and A beta 40 in senile plaques with end-specific A beta monoclonals: evidence that an initially deposited species is A beta 42(43). *Neuron*. **13**, 45-53 (1994).
8. Reinert, J. *et al.* Deposition of C-terminally truncated Aβ species Aβ37 and Aβ39 in Alzheimer's disease and transgenic mouse models. *Acta Neuropathologica Communications*. **4**, 24 (2016).
9. Saido, T.C. *et al.* Dominant and differential deposition of distinct beta-amyloid peptide species, A beta N3(pE), in senile plaques. *Neuron*. **14**, 457-466 (1995).
10. Harigaya, Y. *et al.* Amyloid beta protein starting pyroglutamate at position 3 is a major component of the amyloid deposits in the Alzheimer's disease brain. *Biochemical and Biophysical Research Communications*. **276**, 422-427 (2000).

11. Vinters, H.V. Cerebral amyloid angiopathy. A critical review. *Stroke*. **18**, 311-324 (1987).
12. Saito, T. *et al.* Potent amyloidogenicity and pathogenicity of A $\beta$ 43. *Nature Neuroscience*. **14**, 1023-1032 (2011).
13. Sergeant, N. *et al.* Truncated beta-amyloid peptide species in pre-clinical Alzheimer's disease as new targets for the vaccination approach. *Journal of Neurochemistry*. **85**, 1581-1591 (2003).
14. Suzuki, N. *et al.* High tissue content of soluble beta 1-40 is linked to cerebral amyloid angiopathy. *The American Journal of Pathology*. **145** (2), 452-460 (1994).
15. Miyasaka, T. *et al.* Visualization of newly deposited tau in neurofibrillary tangles and neuropil threads. *Journal of Neuropathology & Experimental Neurology*. **64**, 665-674 (2005).
16. Portelius, E. *et al.* Mass spectrometric characterization of brain amyloid beta isoform signatures in familial and sporadic Alzheimer's disease. *Acta Neuropathologica*. **120**, 185-193 (2010).
17. Kelley, A.R., Perry, G., Castellani, R.J., Bach, S.B. Laser-Induced In-Source Decay Applied to the Determination of Amyloid-Beta in Alzheimer's Brains. *ACS Chemical Neuroscience*. **7**, 261-268 (2016).
18. Stoeckli, M., Staab, D., Staufenbiel, M., Wiederhold, K.H., Signor, L. Molecular imaging of amyloid beta peptides in mouse brain sections using mass spectrometry. *Analytical Biochemistry*. **311**, 33-39 (2002).
19. Stoeckli, M. *et al.* MALDI MS imaging of amyloid. *Methods in Enzymology*. **412**, 94-106 (2006).
20. Seeley, E.H., Caprioli, R.M. Molecular imaging of proteins in tissues by mass spectrometry. *Proceedings of the National Academy of Sciences of the United States of America*. **105**, 18126-18131 (2008).
21. Kakuda, N. *et al.* Distinct deposition of amyloid- $\beta$  species in brains with Alzheimer's disease pathology visualized with MALDI imaging mass spectrometry. *Acta Neuropathologica Communications*. **5**, 73 (2017).
22. Weller, R.O., Djuanda, E., Yow, H.Y., Carare, R.O. Lymphatic drainage of the brain and the pathophysiology of neurological disease. *Acta Neuropathologica*. **117**, 1-14 (2009).
23. Weller, R.O., Boche, D., Nicoll, J.A. Microvasculature changes and cerebral amyloid angiopathy in Alzheimer's disease and their potential impact on therapy. *Acta Neuropathologica*. **118**, 87-102 (2009).

24. Weller, R.O., Subash, M., Preston, S.D., Mazanti, I., Carare, R.O. Perivascular drainage of amyloid-beta peptides from the brain and its failure in cerebral amyloid angiopathy and Alzheimer's disease. *Brain Pathology*. **18**, 253-266 (2008).
25. Morris, A.W. *et al.* Vascular basement membranes as pathways for the passage of fluid into and out of the brain. *Acta Neuropathologica*. **131**, 725-736 (2016).
26. Hawkes, C.A. *et al.* Perivascular drainage of solutes is impaired in the ageing mouse brain and in the presence of cerebral amyloid angiopathy. *Acta Neuropathologica*. **121**, 431-443 (2011).
27. Kakuda, N. *et al.* Equimolar production of amyloid beta-protein and amyloid precursor protein intracellular domain from beta-carboxyl-terminal fragment by gamma-secretase. *Journal of Biological Chemistry*. **281**, 14776-14786 (2006).
28. Matsumura, N. *et al.*  $\gamma$ -Secretase associated with lipid rafts: multiple interactive pathways in the stepwise processing of  $\beta$ -carboxyl-terminal fragment. *Journal of Biological Chemistry*. **289**, 5109-5121 (2014).
29. Morishima-Kawashima, M. *et al.* Effect of apolipoprotein E allele epsilon4 on the initial phase of amyloid beta-protein accumulation in the human brain. *The American Journal of Pathology*. **157**, 2093-2099 (2000).
30. Takami, M. *et al.*  $\gamma$ -Secretase: Successive tripeptide and tetrapeptide release from the transmembrane domain of  $\beta$ -carboxyl terminal fragment. *The Journal of Neuroscience*. **29**, 13042-13052 (2009).
31. Kakuda, N. *et al.* Altered  $\gamma$ -secretase activity in mild cognitive impairment and Alzheimer's disease. *EMBO Molecular Medicine*. **4**, 344-352 (2012).
32. Carlred, L. *et al.* Probing amyloid- $\beta$  pathology in transgenic Alzheimer's disease (tgArcSwe) mice using MALDI imaging mass spectrometry. *Journal of Neurochemistry*. **138**, 469-478 (2016).





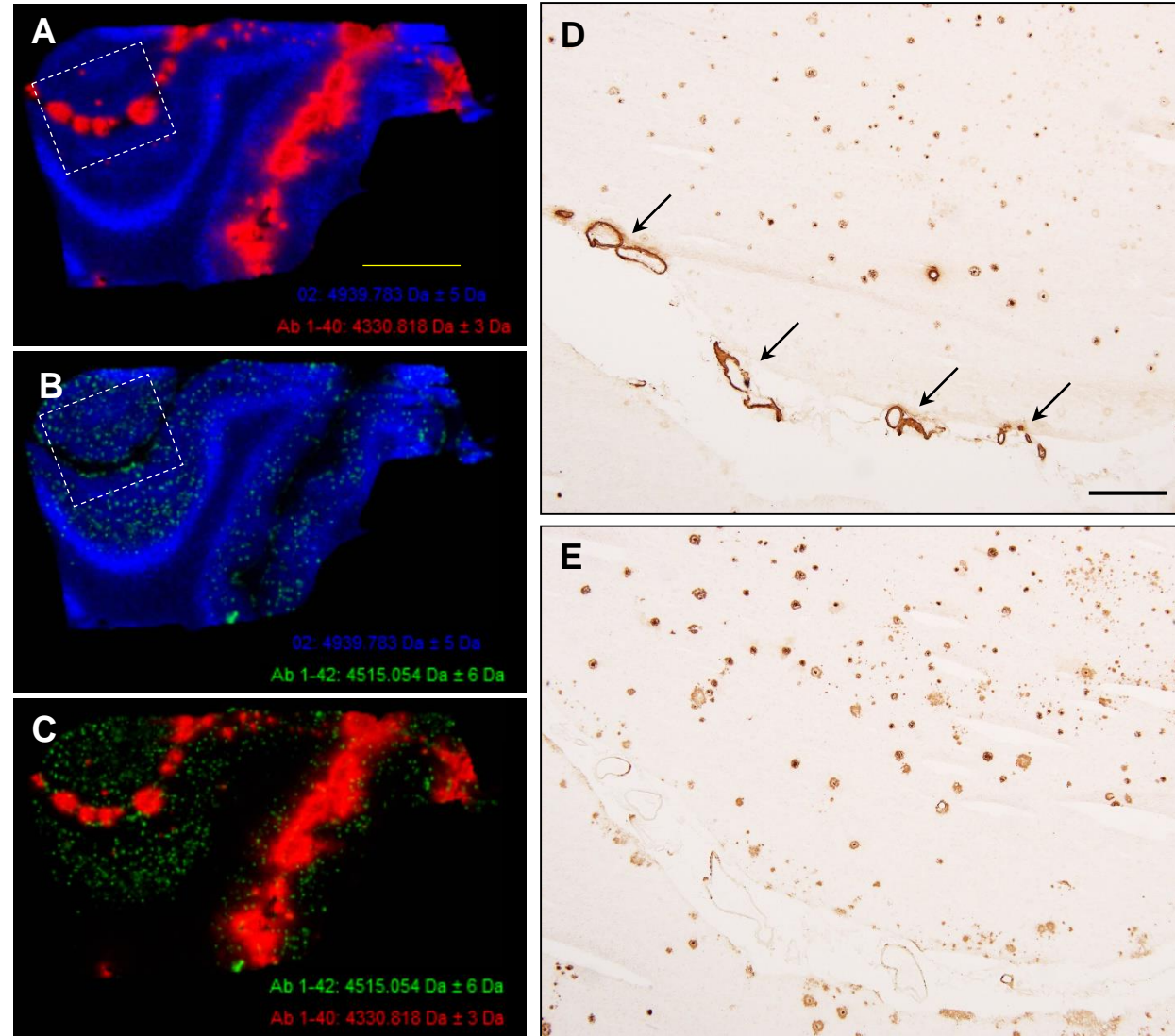




Figure3

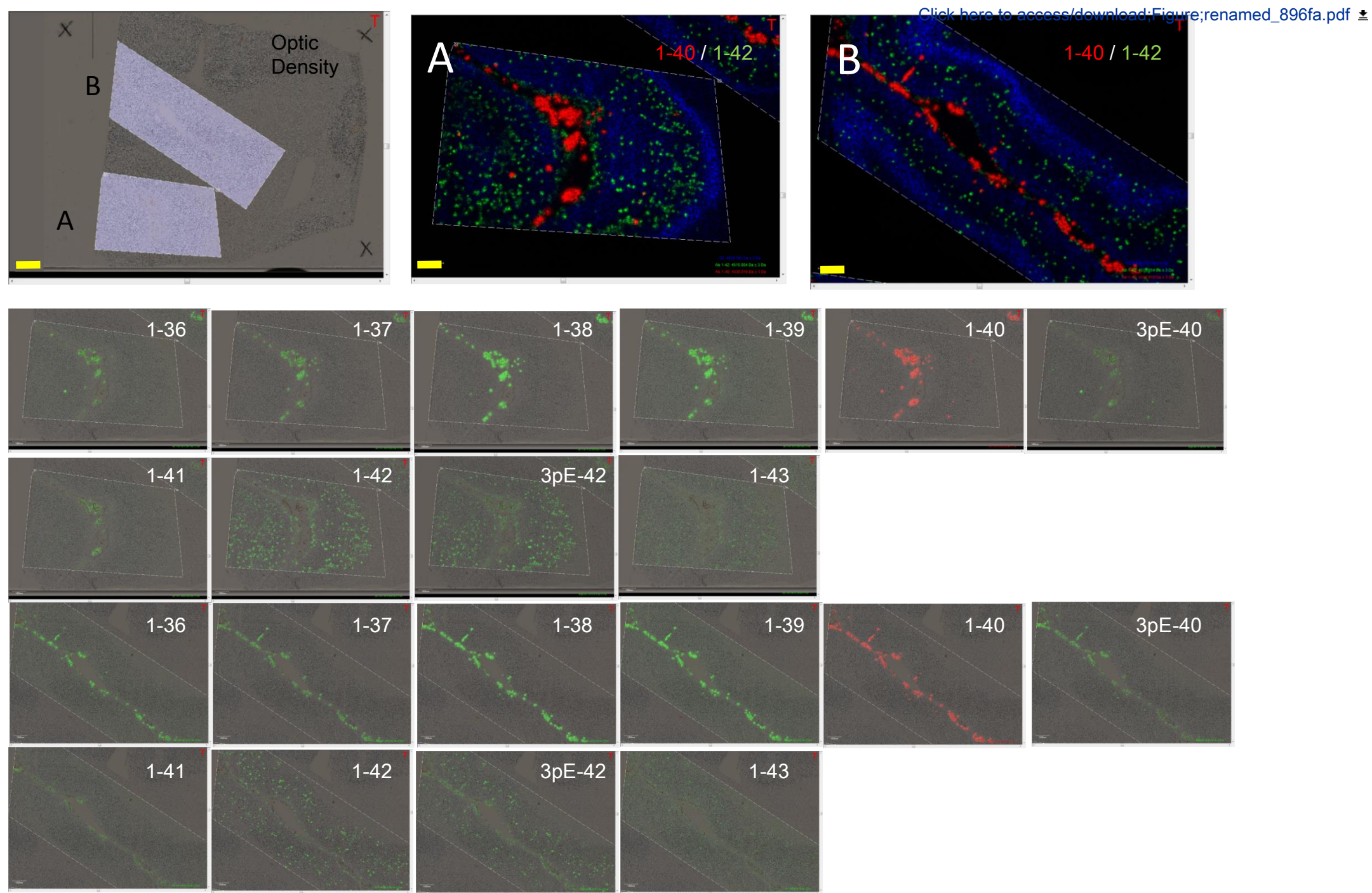




Figure4

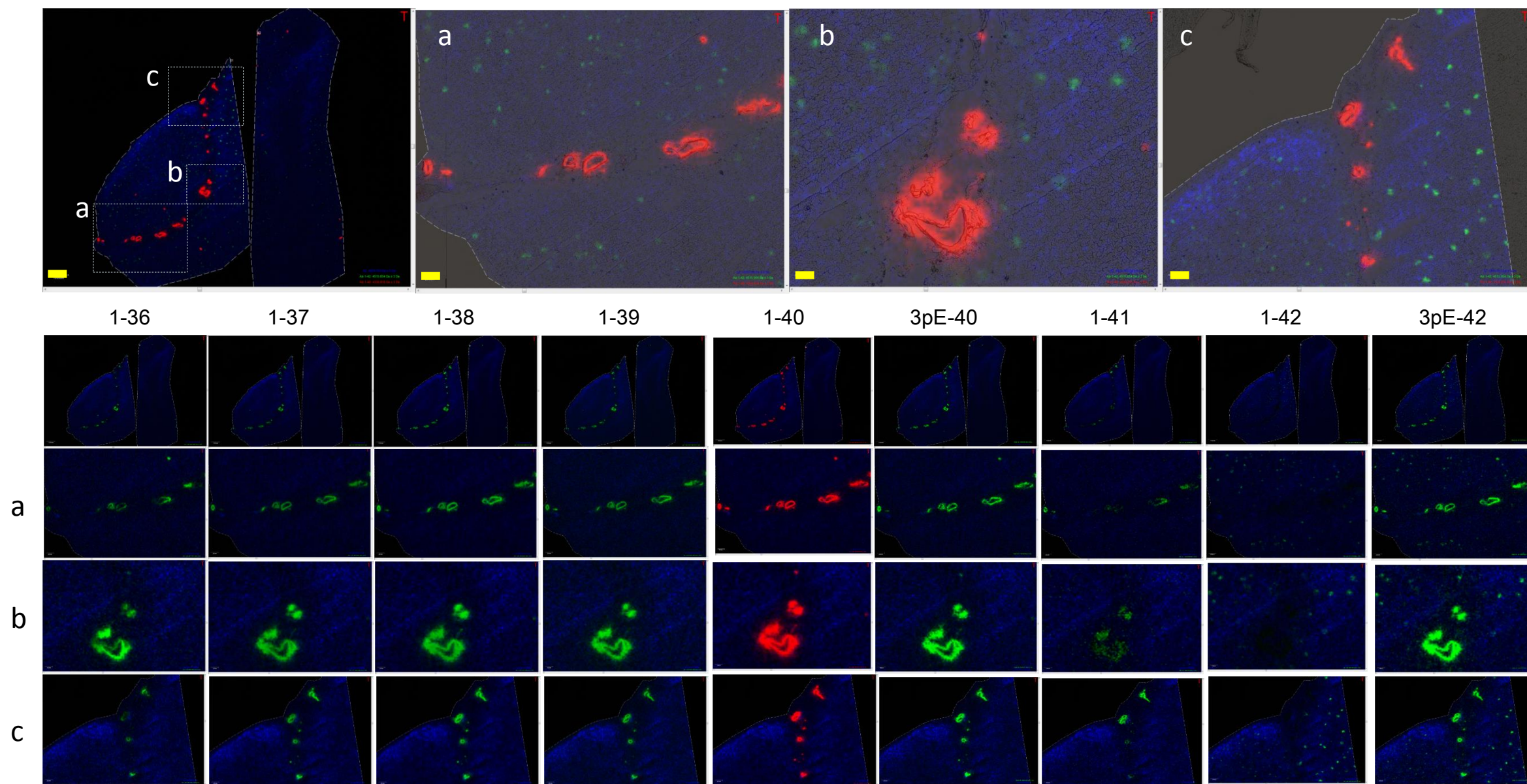


Figure5

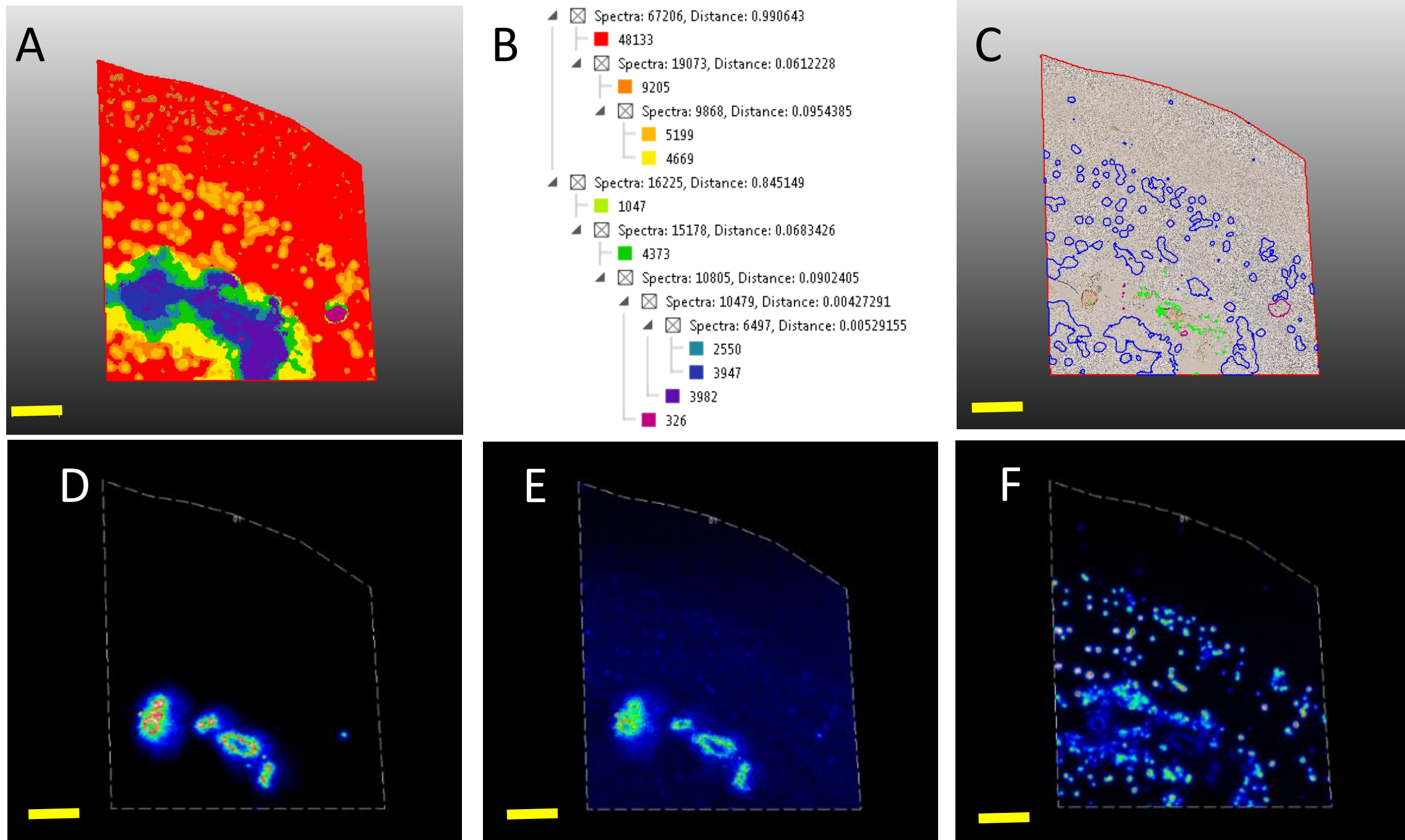


Table 1

Case	Gender	Age at death	Braak SP	CAA
1	M	83	C	0.5
2	M	88	C	1
3	M	84	C	2
4	M	78	C	1
5	M	83	C	1
6	M	84	O	0
7	M	78	O	0
8	M	70	O	0
9	M	73	O	0
10	M	81	O	0



Name	Company
Cryostat	Leica Microsystems, Wetz
Indium tin oxide (ITO)-coated microscope glass slide	Bruker Daltonics
Blade (disposable)	Leica Microsystems, Wetz
O.C.T. Compound	Leica Microsystems, Wetz
Scanner	EPSON
Air-Brush	GSI Creos
Compressor	MRHOBBY
Ultrasonic sprayer	Bruker Daltonics
Automatic sprayer	HTX Technologies
Confocal-laser-scanning-microscope	Carl Zeiss Inc.
Ultra high speed MALDI instrument	Bruker Daltonics
MALDI control software	Bruker Daltonics
Data analysis software	Bruker Daltonics
Molecular histology software	SCiLS, Bremen, Germany
Statistical software	SCiLS, Bremen, Germany
Sinapinic acid (SA)	Nacalai tesque
Alpha-Cyano-4-hydroxyl-cinnamic acid (CHCA)	Wako
Calibration standard	Bruker Daltonics
Biotinylated anti-mouse IgG antibodies	Vector Laboratories, Inc.,
Biotinylated anti-rabbit IgG antibodies	Vector Laboratories, Inc.,
Avidin and biotinylated HRP complex.	Vector Laboratories, Inc.,
3,3-diaminobenzidine (DAB)	Vector Laboratories, Inc.,

Calalog Number	Comments
----------------	----------

CM1950	
--------	--

#237001	
---------	--

#117394	
---------	--

FSC 22 Blue	
-------------	--

GT-980	
--------	--

PS274	
-------	--

Mr.Linear compressor L5	
-------------------------	--

ImagePrep	
-----------	--

TM Sprayer	
------------	--

LSM 700	
---------	--

rapifleX MALDI Tissue typer	
-----------------------------	--

FlexControl 3.8	
-----------------	--

FlexImaging 5.0	
-----------------	--

SciLS Lab 2016a	
-----------------	--

SciLS Lab 2016a	
-----------------	--

30494-91	
----------	--

037-19261	
-----------	--

Burlingame, CA	
----------------	--

Burlingame, CA	
----------------	--

Vectastain Elite ABC kit	
--------------------------	--

Vectastain Elite ABC kit	
--------------------------	--



1 Alewife Center #200  
Cambridge, MA 02140  
tel. 617.945.9051  
www.jove.com

## ARTICLE AND VIDEO LICENSE AGREEMENT

Title of Article:

*Visualization of Amyloid beta Deposits in Human Brain with Matrix-assisted Laser Desorption/Ionization Imaging Mass Spectrometry*

Author(s):

*Masaya Hasegawa, Takashi Nishizawa, Nobuko Kikuchi, Tomohiro Miyasaka, Yuki Kuzuhara, Shigeo Murayama,*

Item 1 (check one box): The Author elects to have the Materials be made available (as described at

http://www.jove.com/author) via: ☒ Standard Access ☐ Open Access

*Yasuo Ihara*

Item 2 (check one box):



The Author is NOT a United States government employee.



The Author is a United States government employee and the Materials were prepared in the course of his or her duties as a United States government employee.



The Author is a United States government employee but the Materials were NOT prepared in the course of his or her duties as a United States government employee.

### ARTICLE AND VIDEO LICENSE AGREEMENT

1. **Defined Terms.** As used in this Article and Video License Agreement, the following terms shall have the following meanings: "Agreement" means this Article and Video License Agreement; "Article" means the article specified on the last page of this Agreement, including any associated materials such as texts, figures, tables, artwork, abstracts, or summaries contained therein; "Author" means the author who is a signatory to this Agreement; "Collective Work" means a work, such as a periodical issue, anthology or encyclopedia, in which the Materials in their entirety in unmodified form, along with a number of other contributions, constituting separate and independent works in themselves, are assembled into a collective whole; "CRC License" means the Creative Commons Attribution-Non Commercial-No Derivs 3.0 Unported Agreement, the terms and conditions of which can be found at: <http://creativecommons.org/licenses/by-nc-nd/3.0/legalcode>; "Derivative Work" means a work based upon the Materials or upon the Materials and other pre-existing works, such as a translation, musical arrangement, dramatization, fictionalization, motion picture version, sound recording, art reproduction, abridgment, condensation, or any other form in which the Materials may be recast, transformed, or adapted; "Institution" means the institution, listed on the last page of this Agreement, by which the Author was employed at the time of the creation of the Materials; "JoVE" means MyJoVE Corporation, a Massachusetts corporation and the publisher of *The Journal of Visualized Experiments*; "Materials" means the Article and / or the Video; "Parties" means the Author and JoVE; "Video" means any video(s) made by the Author, alone or in conjunction with any other parties, or by JoVE or its affiliates or agents, individually or in collaboration with the Author or any other parties, incorporating all or any portion of the Article, and in which the Author may or may not appear.

2. **Background.** The Author, who is the author of the Article, in order to ensure the dissemination and protection of the Article, desires to have the JoVE publish the Article and create and transmit videos based on the Article. In furtherance of such goals, the Parties desire to memorialize in this Agreement the respective rights of each Party in and to the Article and the Video.

3. **Grant of Rights in Article.** In consideration of JoVE agreeing to publish the Article, the Author hereby grants to JoVE, subject to Sections 4 and 7 below, the exclusive, royalty-free, perpetual (for the full term of copyright in the Article, including any extensions thereto) license (a) to publish, reproduce, distribute, display and store the Article in all forms, formats and media whether now known or hereafter developed (including without limitation in print, digital and electronic form) throughout the world, (b) to translate the Article into other languages, create adaptations, summaries or extracts of the Article or other Derivative Works (including, without limitation, the Video) or Collective Works based on all or any portion of the Article and exercise all of the rights set forth in (a) above in such translations, adaptations, summaries, extracts, Derivative Works or Collective Works and (c) to license others to do any or all of the above. The foregoing rights may be exercised in all media and formats, whether now known or hereafter devised, and include the right to make such modifications as are technically necessary to exercise the rights in other media and formats. If the "Open Access" box has been checked in Item 1 above, JoVE and the Author hereby grant to the public all such rights in the Article as provided in, but subject to all limitations and requirements set forth in, the CRC License.

## ARTICLE AND VIDEO LICENSE AGREEMENT

full, unfettered access to the facilities of the Author or of the Author's institution as necessary to make the Video, whether actually published or not. JoVE has sole discretion as to the method of making and publishing the Materials, including, without limitation, to all decisions regarding editing, lighting, filming, timing of publication, if any, length, quality, content and the like.

11. **Indemnification.** The Author agrees to indemnify JoVE and/or its successors and assigns from and against any and all claims, costs, and expenses, including attorney's fees, arising out of any breach of any warranty or other representations contained herein. The Author further agrees to indemnify and hold harmless JoVE from and against any and all claims, costs, and expenses, including attorney's fees, resulting from the breach by the Author of any representation or warranty contained herein or from allegations or instances of violation of intellectual property rights, damage to the Author's or the Author's institution's facilities, fraud, libel, defamation, research, equipment, experiments, property damage, personal injury, violations of institutional, laboratory, hospital, ethical, human and animal treatment, privacy or other rules, regulations, laws, procedures or guidelines, liabilities and other losses or damages related in any way to the submission of work to JoVE, making of videos by JoVE, or publication in JoVE or elsewhere by JoVE. The Author shall be responsible for, and shall hold JoVE harmless from, damages caused by lack of sterilization, lack of cleanliness or by contamination due to the making of a video by JoVE its employees, agents or independent contractors. All sterilization, cleanliness or decontamination procedures shall be solely the responsibility of the Author and shall be undertaken at the Author's

expense. All indemnifications provided herein shall include JoVE's attorney's fees and costs related to said losses or damages. Such indemnification and holding harmless shall include such losses or damages incurred by, or in connection with, acts or omissions of JoVE, its employees, agents or independent contractors.

12. **Fees.** To cover the cost incurred for publication, JoVE must receive payment before production and publication the Materials. Payment is due in 21 days of invoice. Should the Materials not be published due to an editorial or production decision, these funds will be returned to the Author. Withdrawal by the Author of any submitted Materials after final peer review approval will result in a US\$1,200 fee to cover pre-production expenses incurred by JoVE. If payment is not received by the completion of filming, production and publication of the Materials will be suspended until payment is received.

13. **Transfer, Governing Law.** This Agreement may be assigned by JoVE and shall inure to the benefits of any of JoVE's successors and assignees. This Agreement shall be governed and construed by the internal laws of the Commonwealth of Massachusetts without giving effect to any conflict of law provision thereunder. This Agreement may be executed in counterparts, each of which shall be deemed an original, but all of which together shall be deemed to be one and the same agreement. A signed copy of this Agreement delivered by facsimile, e-mail or other means of electronic transmission shall be deemed to have the same legal effect as delivery of an original signed copy of this Agreement.

A signed copy of this document must be sent with all new submissions. Only one Agreement required per submission.

### CORRESPONDING AUTHOR:

Name:

Masaya Ikegawa

Department:

Life and Medical Systems

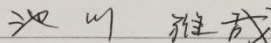
Institution:

Doshisha University

Article Title:

Visualization of Amyloid beta Deposits in Human Brain with Matrix-assisted Laser Desorption/Ionization Imaging mass Spectrometry

Signature:



Date:

2018.4.23.

Please submit a signed and dated copy of this license by one of the following three methods:

- 1) Upload a scanned copy of the document as a pdf on the JoVE submission site;
- 2) Fax the document to +1.866.381.2236;
- 3) Mail the document to JoVE / Attn: JoVE Editorial / 1 Alewife Center #200 / Cambridge, MA 02139

For questions, please email [submissions@jove.com](mailto:submissions@jove.com) or call +1.617.945.9051



**Editorial comments:**

1. We have done some copyediting (see attached manuscript); however there are still some unclear sections. Please see notes in the manuscript.

Thank you for your advice and we followed every comment. Please refer our updated version.

2. There are unfortunately still a few sections in the manuscript that overlap with previous work; please see the attached iThenticate report as well as notes in the manuscript.

In order to avoid overlap with our previous work, we have updated one figure as Figure 5. This is a novel aspect of the current protocol and we have substituted this part from immunohistochemistry.

3. Figure 4: The upper left does not appear to be an optic density figure.

Thank you for this suggestion. We have revised as follows:

*Scale bars indicate 200  $\mu\text{m}$  except upper left optic density figure where scale bars indicate 1 mm.*